

1 Single cell transcriptome sequencing on the Nanopore  
2 platform with ScNapBar

3 Qi Wang<sup>1</sup>, Sven Bönigk<sup>1</sup>, Volker Böhm<sup>2,3</sup>, Niels Gehring<sup>2,3</sup>, Janine Altmüller<sup>4</sup>,  
4 and Christoph Dieterich<sup>\*1,5,6</sup>

5 <sup>1</sup>Klaus Tschira Institute for Integrative Computational Cardiology, University Hospital  
6 Heidelberg, 69120 Heidelberg, Germany

7 <sup>2</sup>Institute for Genetics, University of Cologne, 50674 Köln, Germany

8 <sup>3</sup>Center for Molecular Medicine Cologne (CMMC), University of Cologne, 50937 Köln,  
9 Germany

10 <sup>4</sup>Cologne Center for Genomics (CCG), University of Cologne, Weyertal 115b, 50931  
11 Köln, Germany

12 <sup>5</sup>Department of Internal Medicine III (Cardiology, Angiology, and Pneumology),  
13 University Hospital Heidelberg, 69120 Heidelberg, Germany

14 <sup>6</sup>German Centre for Cardiovascular Research (DZHK)-Partner Site  
15 Heidelberg/Mannheim, 69120 Heidelberg, Germany

16 **Abstract**

17 The current ecosystem of single cell RNA-seq platforms is rapidly  
18 expanding, but robust solutions for single cell and single molecule full-  
19 length RNA sequencing are virtually absent. A high-throughput sol-  
20 ution that covers all aspects is necessary to study the complex life  
21 of mRNA on the single cell level. The Nanopore platform offers long  
22 read sequencing and can be integrated with the popular single cell  
23 sequencing method on the 10x Chromium platform. However, the  
24 high error-rate of Nanopore reads poses a challenge in downstream  
25 processing (e.g. for cell barcode assignment). We propose a solution  
26 to this particular problem by using a hybrid sequencing approach on  
27 Nanopore and Illumina platforms. Our software ScNapBar enables cell  
28 barcode assignment with high accuracy, especially if sequencing satura-  
29 tion is low. ScNapBar uses unique molecular identifier (UMI) or Naïve  
30 Bayes probabilistic approaches in the barcode assignment, depending  
31 on the available Illumina sequencing depth. We have benchmarked the  
32 two approaches on simulated and real Nanopore datasets. We further  
33 applied ScNapBar to pools of cells with an active or a silenced non-  
34 sense mediated RNA decay pathway. Our Nanopore read assignment  
35 distinguishes the respective cell populations and reveals characteristic  
36 nonsense-mediated mRNA decay events depending on cell status.

37 **Keywords:** Bayesian, 10X Genomics, Cell barcode assignment, Nonsense-  
38 mediated mRNA decay (NMD)

---

\*christoph.dieterich@uni-heidelberg.de

## 39 INTRODUCTION

40 Full-length cDNA sequencing allows us to investigate the differential iso-  
41 forms of transcripts, which is especially useful in studying the complex life of  
42 mRNA. Compared to the Illumina sequencing approaches, third-generation  
43 sequencing generates much longer reads and thus avoids artifacts from tran-  
44 scriptome assembly, but often has limitations such as low throughput and  
45 poor base-calling accuracy. Two principal third-generation sequencing plat-  
46 forms exist: Oxford Nanopore Technologies (ONT) and Pacific Biosciences  
47 (PacBio) (Volden et al., 2018). Others and we chose the ONT platform to  
48 study full-length mRNA transcripts due to its better scalability and flex-  
49 ibility (Lebrigand et al., 2020). Full-length transcriptome sequencing can  
50 be taken to the single level by sequencing barcoded 10x Genomics cDNA  
51 libraries. However, this brings about certain challenges, which we address  
52 in our work.

53 First, the native error rate of Nanopore DNA sequencing is < 5% on  
54 the latest R10.3 platform (<http://nanoporetech.com>) as opposed to the  
55 typical Illumina error rate of 0.1%. Due to its high error rate, barcode iden-  
56 tification and assignment are challenging for single-cell sequencing. In the  
57 10X Genomics single-cell protocol, about 99% barcode sequences from Illu-  
58 mina sequencing can be exactly matched to the 16-bp cell barcodes, while  
59 with Nanopore sequencing, the exact matches are less than 50% (0.999<sup>16</sup> vs.  
60 0.95<sup>16</sup>). Many experimental and computational approaches have been devel-  
61 oped to correct Nanopore data. For example, the rolling circle to concate-  
62 meric consensus (R2C2) approach can produce two million full-length cDNA  
63 sequences per MinION flow cell and achieved 98% accuracy (Volden et al.,  
64 2018; Cole et al., 2020; Volden and Vollmers, 2020). Single-cell Nanopore se-  
65 quencing with UMIs (ScNaUmi-seq) can assign cellular barcode with 99.8%  
66 accuracy (Lebrigand et al., 2020). However, R2C2 requires sufficient se-  
67 quencing coverage to call consensus reads, and ScNaUmi-seq requires high  
68 sequencing depth to guarantee an adequate overlap of UMI sequences be-  
69 tween Illumina and Nanopore libraries.

70 On the other hand, end-to-end solutions for barcode demultiplexing and  
71 read quality filtering on the ONT platform are still in its infancy. For ex-  
72 ample, Mandalarion uses BLAT (Kent, 2002) for barcode demultiplexing  
73 (Byrne et al., 2017). Porechop (<https://github.com/rrwick/Porechop>)  
74 uses SeqAn (Döring et al., 2008) for adapter removal and barcode demul-  
75 tiplexing in Nanopore sequencing, but it is based on the best alignment  
76 which could be error-prone. Minibar (Krehenwinkel et al., 2019), Deep-  
77 biner (Wick et al., 2018), and DeePlexiCon (Smith et al., 2020) are only  
78 suitable for multiplexing a few barcoded samples rather than the single-cell  
79 library which contains several thousands of barcodes.

80 Therefore, we developed a software tool called ScNapBar (single-cell  
81 Nanopore barcode demultiplexer) that demultiplexes Nanopore barcodes

82 and is particularly suited for low depth Illumina and Nanopore sequencing.  
83 We evaluated the performance of ScNapBar and demonstrated its high  
84 accuracy in cell barcode assignment for simulated and real Nanopore data.  
85 Our workflow is presented in Fig. 1.

## 86 RESULTS

### 87 Benchmarking the two ScNapBar run modes

88 ScNapBar offers two run modes. The first one uses cell barcode and UMI  
89 information without any additional modeling aspect. The second one in-  
90 troduces a probabilistic model, which performs very well in cases of low  
91 sequencing saturation (i.e. UMI coverage in Illumina data).

#### 92 The UMI approach of ScNapBar

93 The UMI approach requires a matching cell barcodes and UMI tag and  
94 was first developed in Sicelore (Lebrigand et al., 2020). Any cell barcode  
95 predictions that are supported by the presence of both, barcode and UMI  
96 alignment, are very reliable. We performed an *in silico* benchmark of cell  
97 barcode assignment when both, cell barcode and UMI, are found in the  
98 Nanopore read. We observed an average specificity of 99.9% (ScNapBar)  
99 and 99.8% (Sicelore) over 100 averaged simulation runs (Fig. 2a). As ex-  
100 pected, sensitivity heavily depends on Illumina sequencing saturation (Fig.  
101 2a). As the UMI approach relies on consistent genomic mappings for the  
102 Illumina and Nanopore reads, other challenges include: insufficient or in-  
103 accurate genome annotations causing wrong gene assignment; chimeric or  
104 super-long Nanopore reads assigned to multiple genes increase the risk of  
105 assigning a false UMI.

#### 106 The probabilistic approach of ScNapBar

107 Complementary to the UMI approach, we implemented a Bayesian approach  
108 in ScNapBar, which covers the situation of low Illumina sequencing satura-  
109 tion. In our second approach, UMI alignments are no longer used. ScNapBar  
110 evaluates probability scores for each barcode alignment instead. Illumina se-  
111 quencing saturation measures the uniqueness of the transcripts detected in  
112 the Illumina library. Given that we have performed Illumina and Nanopore  
113 sequencing in our approach, the Illumina sequencing saturation limits the  
114 overlap of cell barcodes and UMIs with the low depth Nanopore libraries.  
115 To explore more realistic saturation scenarios, we estimated the Illumina  
116 sequencing saturation for our pilot data set with the Cell Ranger software.  
117 Herein, sequencing saturation is calculated as

$$Saturation = 1 - (n_{deduped\ reads} / n_{reads}) \quad (1)$$

118 where  $n_{deduped\ reads}$  is the number of unique (valid cell-barcode, valid  
119 UMI, gene) combinations among confidently mapped reads and  $n_{reads}$  is the  
120 total number of confidently mapped, valid cell-barcode, valid UMI reads.  
121 For example, we have observed a saturation of 11.3% for our pilot data set.

122 We have simulated one million Nanopore reads with an error model,  
123 which was estimated from our reference Nanopore libraries (see Methods)  
124 using the same gene-barcode-UMI composition as given by the Illumina li-  
125 brary and a sequencing saturation of 100%. We trained a Naïve Bayes clas-  
126 sifier (see Methods) from barcode and adapter alignments of one Nanopore  
127 library, and applied the model for computing the likelihood of the matched  
128 barcodes  $P(r|b_i)$  on the other library. Then we used the frequencies of  
129 the given barcodes in the Illumina library as prior probabilities  $P(b_i)$ , and  
130 calculated the posterior probability  $P(b_i|r)$  from the likelihood and prior  
131 probabilities. We scored each barcode alignment by multiplying the  $P(b_i|r)$   
132 by 100, and assigned the best matching barcode with the highest score  
133 ( $> 50$ ) as predicted barcode assignment. Using the probability scores as  
134 mentioned, ScNapBar correctly assigned 65.8% barcodes from one million  
135 simulated Nanopore reads, of which 26.5% contains at least one mismatch  
136 or indel (Suppl. Fig. S1).

137 We estimate a user data specific error model, simulate data from which  
138 users pick the Bayes score cutoff, which meets their requirements on sensitiv-  
139 ity and specificity, respectively. We inspected the densities of the probability  
140 scores by examining the ground-truth barcodes, and confirmed that the cor-  
141 rect barcode assignments are enriched in high scoring barcodes (Suppl. Fig.  
142 S2b ).

143 Our probabilistic model outperforms Sicelore for cases where UMI infor-  
144 mation is sparse and cannot be used to assign cell barcodes. In the absence  
145 of UMIs, ScNapBar reaches 97.1% specificity while Sicelore only reaches  
146 only 57.1% (Fig. 2b).

147 We examined performance metrics of cell barcode assignment over a  
148 range of score cutoffs (from 1 to 99), and the specificity increases while the  
149 sensitivity decreases along with the increased thresholds (Suppl. Fig. S3).  
150 We pooled the simulated results from FC1 and FC2 together, and use the  
151 Sicelore assignments as baselines. As some cutoff thresholds, ScNapBar has  
152 better F1 scores than Sicelore (e.g., cutoff=50), and ScNapBar score  $>90$  is  
153 as accurate as Sicelore with UMI from the Receiver-Operating Characteristic  
154 (ROC) graph (Fig. 2c).

## 155 The runtime performance of ScNapBar

156 ScNapBar is based on the Needleman-Wunsch algorithm (gap-end free, semi-  
157 global sequence alignment) of FLEXBAR (Dodd et al., 2012; Roehr et al.,  
158 2017) and Sicelore is based on the “brute force approach” which hashes all  
159 possible sequence tag variants (including indels) up to a certain edit distance

160 (2 or 3) of the given barcode sequences. The time complexity of ScNapBar  
161 and Sicelore can be represented as Eq. 2a and Eq. 2b, respectively.

$$T(n) \propto (l_{pos} + l_{cb})l_{cb}n_{cb} \quad (2a)$$

$$T(n) \propto \frac{(n_{pos} + l_{cb})!}{n_{ed}!}l_{pos}n_{cb} \quad (2b)$$

162 where  $n_{pos}$  is the number of nucleotides downstream of the adapter, and  
163  $l_{pos} = 2n_{pos} + 1$  as Sicelore typically searches the same number of nucleotides  
164 upstream and downstream of the ending position of the adapter.  $n_{cb}$  stands  
165 for the number of barcodes in the whitelist from Illumina sequencing.  $n_{ed}$   
166 is typically two or three as larger edit distances increase runtime drastically  
167 and are not necessary due to the increasing error rate.  $l_{cb}$  is the length of  
168 the barcode and is 16 in this study.

169 We compared the runtime between ScNapBar and Sicelore with regards  
170 to start positions of barcodes (number of nucleotides between adapter and  
171 barcode). We discovered that Sicelore may be orders of magnitude slower  
172 than ScNapBar given the same search space (2,052 cellular barcodes, edit  
173 distance=3), but also its runtime increases exponentially as the barcode start  
174 position increases (Fig. 3b). Therefore, the default setting in Sicelore only  
175 searches  $\pm 1$ -nt from the end of the adapter, which may limit the nucleotides  
176 to search and cause false positives. We created 2x2 contingency tables of  
177 the number of correct and false assignments caused by various factors (e.g.,  
178 indels  $\geq 3$  against  $< 3$ ), and performed Fisher's test. The results showed  
179 that the odds ratio of "barcode start position  $\geq 3$ " from Sicelore is 24.8,  
180 while the odds ratio of the same test from ScNapBar is only 0.14 (Suppl.  
181 Table S1). This implies allowing more nucleotides from the start of the  
182 barcode can effectively reduce the false-positive rate, which is feasible using  
183 less time with ScNapBar.

184 We also performed real runtime comparison on barcode assignment on  
185 the previously simulated one million Nanopore reads. In this test, we pro-  
186 vided ScNapBar ten barcode white lists which contain from 1,000 to 10,000  
187 most abundant barcodes, and ScNapBar's runtime is only dependent on the  
188 number of barcodes to search given the other factors are fixed in this study  
189 (Fig. 3a). Then we tested Sicelore with searching parameters of barcode  
190 edit distance between two and three, barcode start position from  $\pm 2$  bp to  
191  $\pm 4$  bp, and UMI edit distance of 0. ScNapBar requires only one-fifth CPU  
192 time than Sicelore when  $\pm 4$  bp barcode start position and three barcode  
193 edit distance are considered in both programs (Fig. 3b).

194 **The performance of ScNapBar on the real data**

195 **The performance of ScNapBar on an Illumina library with high**  
196 **sequencing saturations**

197 We tested our ScNapBar software with the UMI approach (option 1) on the  
198 dataset from the Sichelore paper (NCBI GEO GSE130708). Herein, Illumina  
199 sequencing saturation reaches 90.5%. We extracted the UMI whitelists for  
200 each gene or genomic window (500bp) from the Illumina library, and set the  
201 minimum length of UMI match to 7 in ScNapBar. Sichelore and ScNapBar  
202 assigned barcodes to 84.3% and 77.2% of the 9,743,819 Nanopore reads  
203 (Suppl. Fig. S4), respectively. 88.4% of the assigned barcodes are identical.

204 **The performance of ScNapBar on an Illumina library with low**  
205 **sequencing saturations**

206 We ran ScNapBar with the Bayesian approach (option 2) on our NMD  
207 dataset, which only has an Illumina saturation of 11.3%. ScNapBar assigns  
208 35.0% and 36.3% of the Nanopore reads to cell barcodes with probabil-  
209 ity score >50, while Sichelore assigns 40.8% and 42.5% without using UMIs  
210 (“Assigned to barcode” in Fig. 5) and only assigns 4.0% and 4.2% of the  
211 Nanopore reads using the UMI approach for FC1 and FC2, respectively.  
212 Based on our previous simulations, we estimate that a greater proportion  
213 (also by absolute numbers) of ScNapBar assignments are correct (“Correctly  
214 assigned” in Fig. 5).

215 **Single cell clustering and splicing in a pool of wildtype and NMD**  
216 **mutant cells.**

217 Although alternative splicing increases the coding potential of the human  
218 genome, aberrant isoforms are frequently generated that contain premature  
219 termination codons (PTCs) (Lewis et al., 2003). Regular stop codons are  
220 normally located in the last exon of a transcript or at least 50 nucleotides up-  
221 stream of the last exon-exon junction (Lindeboom et al., 2019). Alternative  
222 splicing can result in PTCs by exon inclusion/exclusion events or can convert  
223 normal stop codons into PTCs by splicing in the 3' UTR. Transcripts har-  
224 boring PTCs are rapidly degraded by the nonsense-mediated mRNA decay  
225 (NMD) machinery, not only to remove faulty mRNAs, but also to fine-tune  
226 and regulate the transcriptome. 5-40% of all expressed human genes are di-  
227 rectly or indirectly altered in expression levels, splicing pattern, or isoform  
228 composition by the NMD pathway (Boehm et al., 2020). We have sequenced  
229 a pool of NMD active and inactive cells and expect to see an enrichment of  
230 transcripts with PTCs in GFP- cells.

231 We use the GFP label as an independent confirmation of cellular NMD  
232 status and pooled data from both experiments (FC1 and FC2). For the

233 Nanopore data, Seurat identifies 13,807 expressed genes across 1,850 cells.  
234 We extracted the GFP+ barcodes from the Illumina reads mapping, and  
235 rendered the corresponding cells in different colors in the t-SNE plots (Fig.  
236 4). The locations of the GFP+ cells appear in distinct sub-clusters in the  
237 Illumina and Nanopore t-SNE plots.

238 We characterized the structural changes of the assembled Nanopore tran-  
239 scripts based on our customized transcriptome annotations using NMD Clas-  
240 sifier (Hsu et al., 2017). The pool of *SMG7*-KO/*SMG6*-KD (GFP-) cells  
241 harbors almost twice as many inclusion/exclusion events, which lead to the  
242 formation of a PTC (Suppl. Fig. S9a). We quantified the expression level  
243 of 14,185 known NMD transcripts annotated by Ensembl release 101. Af-  
244 ter removing the non-expressed transcripts from the both flow cell runs,  
245 the remaining 6,423 NMD transcripts have shown significantly higher NMD  
246 transcript expression in the *SMG7*-KO/*SMG6*-KD (GFP-) cells than the  
247 WT (GFP+) cells (Suppl. Fig. S9b). We reason that the lowered NMD  
248 response is clearly visible by the enrichment of PTC-containing transcripts  
249 in the pool of *SMG7*-KO/*SMG6*-KD (GFP-) cells. Consequently, the cell  
250 barcode assignments meet our "biological" expectations.

251 We investigated a well-established NMD target *SRSF2* in detail (Sureau  
252 et al., 2001). The wildtype isoforms are present in both GFP+/- cells, while  
253 in the GFP- cells, the PTC-containing isoforms are more abundant in the  
254 GFP- cells (Suppl. Fig. S10a). The view on the *SRSF2* genome locus  
255 confirmed the different splicing junctions between two cell types (Suppl.  
256 Fig. S10b). The inclusion of exon 3 (middle) is clearly favored GFP- cells.

## 257 DISCUSSION

258 The current ecosystem of single-cell RNA-seq platforms is rapidly expand-  
259 ing, but robust solutions for single-cell and single-molecule full-length RNA  
260 sequencing are virtually absent. In our manuscript, we combined Oxford  
261 Nanopore single-molecule sequencing of 10x Genomics cDNA libraries and  
262 developed a novel software tool to arrive at single-cell, single-molecule, full  
263 cDNA length resolution. In contrast to Lebrigand et al. (2020), our Bayesian  
264 method for cell barcode assignment performs superior in situation of low se-  
265 quencing saturation. We could track in a well-controlled setting, i.e. by  
266 using GFP labeled cells and strong transcriptome perturbations, full-length  
267 transcript information at a single-cell level. We have identified differential  
268 RNA splicing linked to NMD pathway activity across our cell population.  
269 Our high-throughput full-length RNA sequencing solution is a necessary  
270 step forward towards studying the complex life of mRNA on single-cell level.  
271 This opens up unprecedented opportunities in low saturation settings such  
272 as multiplexed CRISPR-based screens.

## 273 MATERIALS AND METHODS

### 274 Single cell samples preparation and experiment

275 We performed an experiment using two different Flp-In-T-REx-293 cell lines:  
276 the wild type cell line with stably integrated FLAG-emGFP and a *SMG7*  
277 knockout (KO) cell line (generated and established in Boehm et al. (2020)).  
278 Wild type cells (GFP+) were transfected with siRNA against Luciferase and  
279 the *SMG7* KO cells (GFP-) were transfected with an siRNA against *SMG6*.  
280 Two days after siRNA transfection, we mixed both cell types at a 1:1 ratio  
281 with a target of 2,000 cells in total. A cDNA library was prepared according  
282 to the 10x Genomics Chromium Single Cell 3' Reagent Kit User Guide (v3  
283 Chemistry) from the pool of cells. The final libraries contain the P5 and  
284 P7 primers. The P5 read contains 21-nt adaptor sequence, 16-nt cellular  
285 barcode, 12-nt UMI, and polyA-tail, followed by cDNA sequences.

### 286 Illumina reads processing and identification of cellular bar- 287 codes

288 We used 10X Genomics Cell Ranger 3.1 (<https://github.com/10XGenomics/cellranger>) to map the Illumina reads onto the reference genome. In  
289 our NMD dataset, the DNA sequences of luciferase were appended to the  
290 reference genome, and therefore the GFP+ cells can be called from Cell  
291 Ranger. Cell Ranger also corrects the sequencing errors in the barcode and  
292 unique molecular identifier (UMI) sequences. Cell Ranger estimates the  
293 number of cells using a Good-Turing frequency estimation model (<https://support.10xgenomics.com>), and characterized the identified barcodes  
294 into the cell-associated and background-associated barcodes. We used the  
295 cell-associated barcode sequences as the cellular barcode whitelist in the fol-  
296 lowing analyses. Our CellRanger analysis estimated 2,052 sequenced cells  
297 (Suppl. Table S2).

### 300 Nanopore reads processing, mapping, and gene assignment

301 We sequenced the two independently prepared Nanopore libraries from the  
302 same cDNA on two Nanopore R9.4 GridION flow cells (FC1 and FC2).  
303 The base-calling of Nanopore reads was done using Guppy v3.3.3, resulting  
304 in 13,126,013 and 11,923,896 reads, respectively. We aligned the Nanopore  
305 reads onto the corresponding reference genome using minimap2 v2.17 (Li,  
306 2018) in the spliced alignment mode (-ax splice). The two Nanopore runs  
307 yielded 11,158,994 and 10,164,820 mappable reads, respectively. We further  
308 assigned gene names to Nanopore reads using the “TagReadWithGeneExon”  
309 program from the Drop-seq tools (Macosko et al., 2015). We assembled all  
310 the Nanopore reads and extended transcriptome annotations using StringTie

311 v2.1.1 (Pertea et al., 2015). The FPKM level of the assembled transcripts  
312 were quantified using Ballgown v2.14.1 (Frazee et al., 2015).

313 **Identification of the adapter, barcode, UMI, and polyA-tail**  
314 **sequences from Nanopore reads**

315 We removed the cDNA sequences from Nanopore reads, and extracted up  
316 to 100bp from both ends. We developed a modified version of FLEXBAR  
317 (Dodd et al., 2012; Roehr et al., 2017) to align P1 primer adapter sequence  
318 with the following parameters (“-ao 10 -ae 0.3 -ag -2 -hr T -hi 10 -he 0.3  
319 -be 0.2 -bg -2 -bo 5 -ul 26 -kb 3 -fl 100”). Then we aligned the Nanopore  
320 reads that have valid adapters to the cellular barcodes which have been  
321 previously identified by Cell Ranger. We scanned the poly-A sequences using  
322 the homopolymer-trimming function of FLEXBAR downstream of the cell  
323 barcode. Once the poly-A sequences were found, the UMI sequences between  
324 the poly-A and barcode were searched using MUMmer 4.0 (Marçais et al.,  
325 2018) (with parameters “-maxmatch -b -c -l 7 -F”) and in-house scripts  
326 against the Illumina UMIs of the same cell and the same gene or genomic  
327 regions ( $\pm$  500bp from each end of the reads). In the end, ScNapBar output  
328 the alignment score of the adapter, the number of mismatches and indel  
329 from the barcode alignment, the length of poly-A and UMI sequences, as  
330 well as the length of the gap between the barcode and adapter. We use  
331 these features to estimate the likelihood of the barcode assignment in the  
332 following steps (Fig. 1).

333 **Simulation and engineering of discriminative features from**  
334 **the barcode and adapter alignments**

335 We characterized the correct and false barcode assignment by simulating  
336 Nanopore reads. We created some artificial template sequences which con-  
337 tain only the P1 primer, cellular barcode, and UMI sequences at the same  
338 frequencies as the Illumina library, followed by 20bp oligo-dT and 32bp  
339 cDNA sequences. In the next step, we first used NanoSim (Yang et al., 2017)  
340 to estimate the error profile of our Nanopore library, then we generated one  
341 million Nanopore reads from the artificial template using the NanoSim sim-  
342 ulator with the previously estimated error profile. We aligned the simulated  
343 Nanopore reads to the adapter and barcode sequences using ScNapBar. We  
344 compared the sequences in the simulated Nanopore reads and the sequences  
345 from the artificial template, and labeled the assigned barcode as correct or  
346 false accordingly. By comparing sequence and alignment features of correct  
347 and false assignments, we found that the two categories (false, true) could  
348 be discriminated by these features (Suppl. Fig. S8c). We then assessed  
349 the importance of each feature towards the correctness of the assignment  
350 (Suppl. Fig. S8a). As these features are uncorrelated (Suppl. Fig. S8b),

351 we train a Naïve Bayes model from these features to predict the likelihood  
352 of the correctness of a barcode assignment.

353 **Calculate cell barcode posterior probability using prior prob-**  
354 **abilities from the Illumina data set**

355 We denote  $b_1, b_2, \dots, b_n$  as barcodes that match to read  $r$  and define  $P(b_1|r)$   
356 as the probability that barcode  $b_1$  was sequenced given  $r$  is observed. Fol-  
357 lowing Bayes' theorem,  $P(b_1|r)$  could be computed as in Eq. 3a, and further  
358 computed as in Eq. 3b according to the total probability theorem.

$$P(b_1|r) = \frac{P(r|b_1)P(b_1)}{P(r)} \quad (3a)$$

$$= \frac{P(r|b_1)P(b_1)}{P(r|b_1)P(b_1) + \dots + P(r|b_n)P(b_n)} \quad (3b)$$

359 where  $P(r|b_1)$  and  $P(r|b_n)$  are computed by the Naïve Bayes predictor,  
360 and priors  $P(b_1)$  and  $P(b_n)$  can be estimated from the observed barcode  
361 counts in Illumina sequencing. For practical reasons, as the probabilities  
362 for the unaligned barcodes that contain a lot of mismatches are pretty low,  
363 we add a pseudocount of 1 to the denominator to represent them. Because  
364 we have sequenced the same library twice using the Nanopore and Illumina  
365 sequencer, we assume prior probabilities  $P(b)$  are the same for the Nanopore  
366 and the Illumina platform (Suppl. Fig. S2a).

367 **Quality assessment and clustering of the single-cell libraries**

368 A meta gene body coverage analysis confirmed the near full-length character  
369 of the Nanopore approach (Suppl. Fig. S6a). After assigning gene names  
370 and cell barcodes to the Nanopore reads, we processed the gene-barcode  
371 expression matrix using Seurat v3.1.1 (Butler et al., 2018) by keeping the  
372 genes expressed in minimal three cells, and cells with more than 200 genes  
373 expressed. We then scaled the expression matrix by a factor of 10,000 and  
374 log-normalized, and performed the t-SNE analysis.

375 **DATA DEPOSITION**

376 All sequencing data were deposited in NBCI's SRA database (accession  
377 number ). ScNapBar workflow (code and tutorial) is available at <https://github.com/dieterich-lab/single-cell-nanopore>.

379 **AUTHOR'S CONTRIBUTIONS**

380 QW implemented the ScNapBar workflow, performed data analyses and  
381 wrote the manuscript. SB modified the FLEXBAR implementation. VB

382 performed cell culture experiments and helped to draft the manuscript. NG  
383 helped to draft the manuscript and acquired funding. JA performed all  
384 sequencing experiments and helped to draft the manuscript. CD super-  
385 vised the project, performed data analyses, acquired funding and wrote the  
386 manuscript.

## 387 ACKNOWLEDGMENTS

388 The authors would like to thank Etienne Boileau, Thiago Britto Borges,  
389 Tobias Jakobi for proof-reading and comments. The authors are grateful  
390 to Marek Franitza for running the experiments on the 10x platform and to  
391 Christian Becker for running ONT sequencing. Supported by Informatics  
392 for Life funded by the Klaus Tschira Foundation.

## 393 REFERENCES

394 Boehm V, Kueckelmann S, Gerbracht JV, Britto-Borges T, Altmüller J,  
395 Dieterich C, and Gehring NH. 2020. Nonsense-mediated mRNA decay  
396 relies on “two-factor authentication” by SMG5-SMG7. *bioRxiv* .

397 Butler A, Hoffman P, Smibert P, Papalexi E, and Satija R. 2018. Integrating  
398 single-cell transcriptomic data across different conditions, technologies,  
399 and species. *Nature Biotechnology* .

400 Byrne A, Beaudin AE, Olsen HE, Jain M, Cole C, Palmer T, DuBois RM,  
401 Forsberg EC, Akeson M, and Vollmers C. 2017. Nanopore long-read  
402 RNAseq reveals widespread transcriptional variation among the surface  
403 receptors of individual B cells. *Nature Communications* .

404 Cole C, Byrne A, Adams M, Volden R, and Vollmers C. 2020. Complete  
405 characterization of the human immune cell transcriptome using accurate  
406 full-length cDNA sequencing. *Genome Research* .

407 Dodt M, Roehr JT, Ahmed R, and Dieterich C. 2012. FLEXBAR-flexible  
408 barcode and adapter processing for next-generation sequencing platforms.  
409 *Biology* .

410 Döring A, Weese D, Rausch T, and Reinert K. 2008. SeqAn an efficient,  
411 generic C++ library for sequence analysis. *BMC Bioinformatics* .

412 Frazee AC, Pertea G, Jaffe AE, Langmead B, Salzberg SL, and Leek JT.  
413 2015. Ballgown bridges the gap between transcriptome assembly and  
414 expression analysis.

415 Hsu MK, Lin HY, and Chen FC. 2017. NMD Classifier: A reliable and  
416 systematic classification tool for nonsense-mediated decay events. *PLoS*  
417 *ONE* .

418 Kent WJ. 2002. BLAT—The BLAST-Like Alignment Tool. *Genome Re-*  
419 *search* .

420 Krehenwinkel H, Pomerantz A, Henderson JB, Kennedy SR, Lim JY, Swamy  
421 V, Shoobridge JD, Graham N, Patel NH, Gillespie RG, et al.. 2019.  
422 Nanopore sequencing of long ribosomal DNA amplicons enables portable  
423 and simple biodiversity assessments with high phylogenetic resolution  
424 across broad taxonomic scale. *GigaScience* .

425 Lebrigand K, Magnone V, Barbry P, and Waldmann R. 2020. High through-  
426 put error corrected Nanopore single cell transcriptome sequencing. *Nature*  
427 *communications* **11**: 4025.

428 Lewis BP, Green RE, and Brenner SE. 2003. Evidence for the widespread  
429 coupling of alternative splicing and nonsense-mediated mRNA decay in  
430 humans. *Proceedings of the National Academy of Sciences of the United*  
431 *States of America* .

432 Li H. 2018. Minimap2: Pairwise alignment for nucleotide sequences. *Bioin-*  
433 *formatics* .

434 Lindeboom RGH, Vermeulen M, Lehner B, and Supek F. 2019. The impact  
435 of nonsense-mediated mRNA decay on genetic disease, gene editing and  
436 cancer immunotherapy. *Nature genetics* **51**: 1645–1651.

437 Macosko EZ, Basu A, Satija R, Nemesh J, Shekhar K, Goldman M, Tirosh  
438 I, Bialas AR, Kamitaki N, Martersteck EM, et al.. 2015. Highly par-  
439 allel genome-wide expression profiling of individual cells using nanoliter  
440 droplets. *Cell* .

441 Marçais G, Delcher AL, Phillippy AM, Coston R, Salzberg SL, and Zimin A.  
442 2018. MUMmer4: A fast and versatile genome alignment system. *PLoS*  
443 *Computational Biology* .

444 Pertea M, Pertea GM, Antonescu CM, Chang TC, Mendell JT, and Salzberg  
445 SL. 2015. StringTie enables improved reconstruction of a transcriptome  
446 from RNA-seq reads. *Nature Biotechnology* .

447 Roehr JT, Dieterich C, and Reinert K. 2017. Flexbar 3.0 - simd and multi-  
448 core parallelization. *Bioinformatics (Oxford, England)* **33**: 2941–2942.

449 Smith MA, Ersavas T, Ferguson JM, Liu H, Lucas MC, Begik O, Bojarski  
450 L, Barton K, and Novoa EM. 2020. Molecular barcoding of native RNAs  
451 using nanopore sequencing and deep learning. *Genome research* **30**: 1345–  
452 1353.

453 Sureau A, Gattoni R, Dooghe Y, Stévenin J, and Soret J. 2001. SC35  
454 autoregulates its expression by promoting splicing events that destabilize  
455 its mRNAs. *EMBO Journal* .

456 Volden R, Palmer T, Byrne A, Cole C, Schmitz RJ, Green RE, and Vollmers  
457 C. 2018. Improving nanopore read accuracy with the R2C2 method en-  
458 ables the sequencing of highly multiplexed full-length single-cell cDNA.  
459 *Proceedings of the National Academy of Sciences of the United States of*  
460 *America* .

461 Volden R and Vollmers C. 2020. Highly Multiplexed Single-Cell Full-Length  
462 cDNA Sequencing of human immune cells with 10X Genomics and R2C2.  
463 *bioRxiv* .

464 Wick RR, Judd LM, and Holt KE. 2018. Deepbinner: Demultiplexing bar-  
465 coded Oxford Nanopore reads with deep convolutional neural networks.  
466 *PLoS Computational Biology* .

467 Yang C, Chu J, Warren RL, and Birol I. 2017. NanoSim: Nanopore sequence  
468 read simulator based on statistical characterization.

469 **FIGURES**

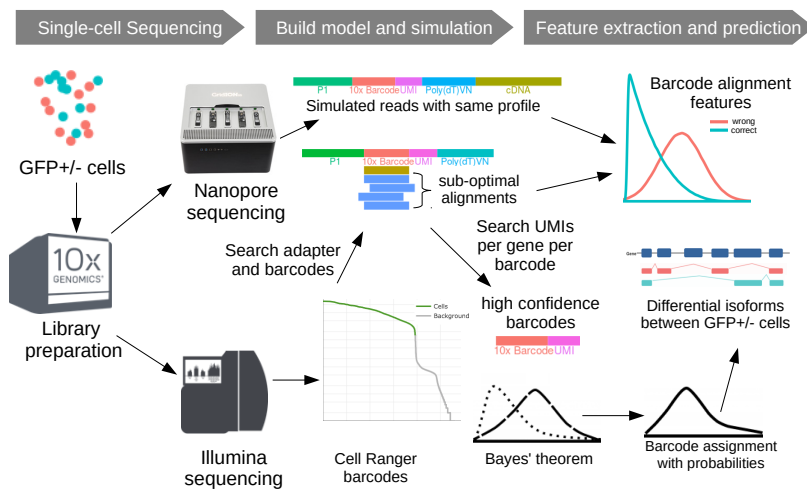
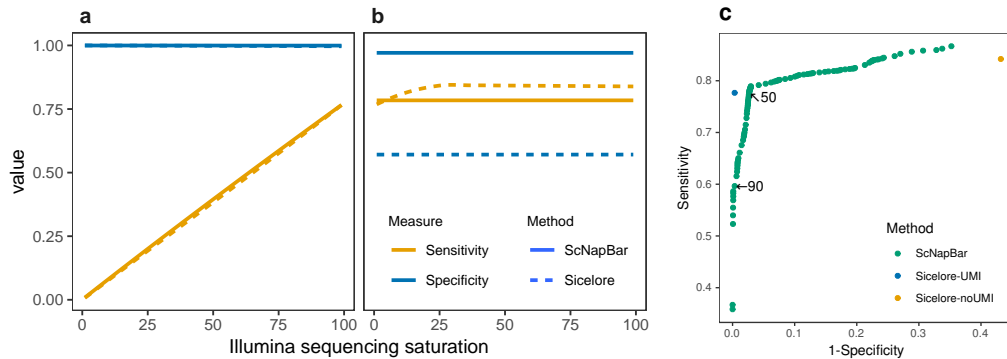
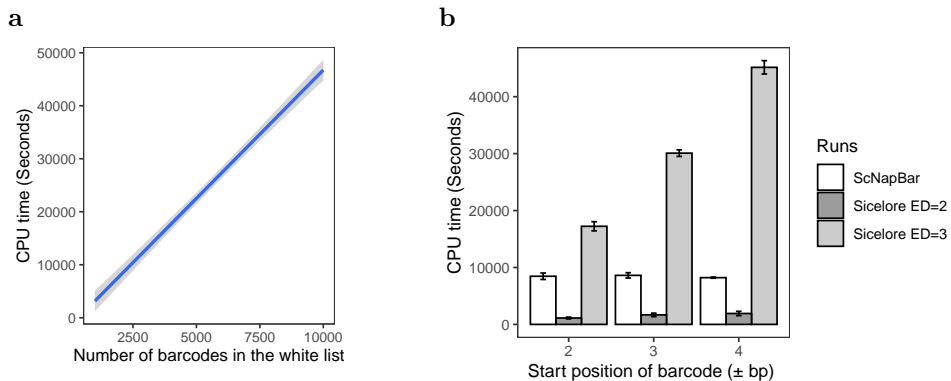


Figure 1: **Combined Single-cell Illumina and Nanopore sequencing strategy.** GFP $^{+/-}$  cells are pooled and sequenced on the Illumina and Nanopore platform. The Nanopore platform generates long cDNA sequencing read that are used in barcode calling and estimating read error parameters. The Illumina data are used to estimate the total number of cells in sequencing and the represented cell barcodes. The simulated data are then used to parameterize a Bayesian model of barcode alignment features to discriminate correct vs. false barcode assignments. This model is then used on the real data to assign cell barcodes to Nanopore reads. The GFP label and known NMD transcripts can be used to validate this assignment.



**Figure 2: Sensitivity and specificity of ScNapBar and Sicelore on 100 Illumina libraries with different levels of saturation.** (a) Bar-code assignment with UMI matches. (b) Bar-code assignment without UMI matches (ScNapBar score  $>50$ ). (c) Benchmark of the specificity and sensitivity of the Illumina library with 100% saturation. We compared the barcode assignments with ScNapBar score  $>1-99$ , and the assignments from Sicelore with UMI support are roughly equivalent to the ScNapBar score  $>90$ .



**Figure 3: Sicelore and ScNapBar CPU time comparison.** (a) ScNapBar CPU time depends on the number of whitelist barcodes (allowing an edit distance of  $>2$  and an offset of up to 4bp between adapter and barcode). Gray area represents the standard deviation for 10 runs. (b) Comparison of ScNapBar and Sicelore CPU times. Benchmark was measured using one million barcode sequences and 2,052 barcodes in the whitelist.

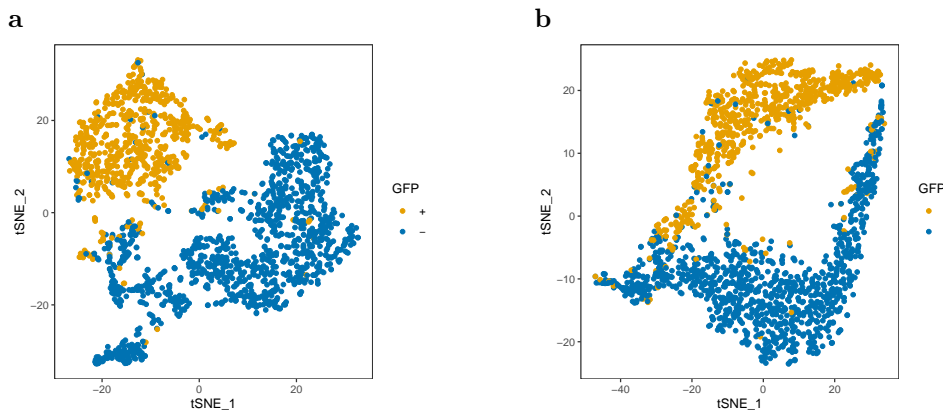


Figure 4: The t-SNE plots of gene-cell matrices. (a) Illumina. (b) Nanopore.

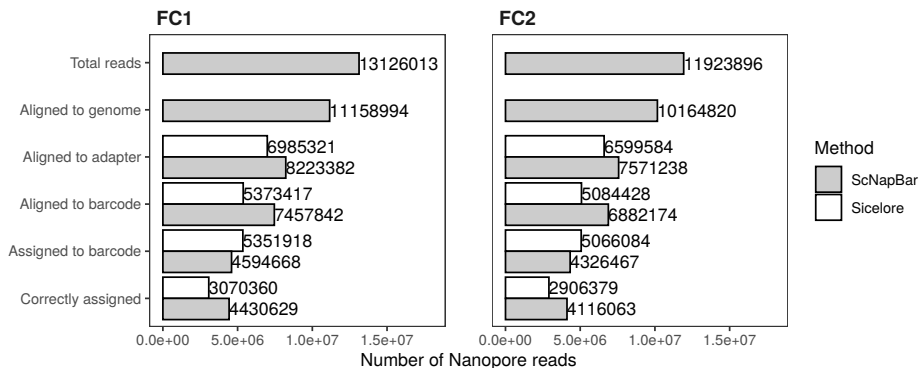


Figure 5: Number of the Nanopore reads identified by ScNapBar and Sicelore from each step. The number of the correctly assigned reads is calculated from the specificity of the assignment in the simulation.

